Soft Matter

PAPER

View Article Online
View Journal | View Issue

Cite this: *Soft Matter*, 2025, **21**, 3814

Structural interplay in block copolymer-bile salt complexes: from globules to ribbons†

Suelen Gauna Trindade,[ab] Guanqun Du,‡[a] Luciano Galantini,[c] Lennart Piculell,[a] Watson Loh*[b] and Karin Schillén*[a]

Received 29th January 2025,
Accepted 9th April 2025

DOI: 10.1039/d5sm00097a

rsc.li/soft-matter-journal

The supramolecular structures resulting from the complexation between the neutral–cationic block copolymer poly(ethylene oxide)-*block*-poly(2-(trimethylammonium)ethyl methacrylate iodide) (PEO_{114}-*b*-$PTMAEMAI_{95}$) and the bile salt sodium deoxycholate (NaDC) were investigated by dynamic light scattering, small-angle X-ray scattering, cryogenic transmission electron microscopy and proton NMR techniques. Complexes were produced using different preparation protocols: the direct mixing of the pure solutions of block copolymer and bile salt, containing their respective simple counterions, and the dispersion in water of a freeze-dried complex salt, free of simple counterions. While the direct mixing protocol produced a mixture of ordered ribbon-like aggregates and globular particles with disordered cores, the complex salt protocol yielded exclusively ordered "ribbons". The globular particles resembled classical spherical "complex coacervate core micelles" with a core of anionic deoxycholate micelles complexed with cationic PTMAEMA(+) blocks, the core radius being limited by the PTMAEMA contour length, and a shell composed of neutral PEO blocks. The drastically different ribbon morphology was found to result from (1) the organization of DC anions into hexagonally packed helices in the core and (2) the limitations on the ribbon thickness imposed by the lengths of the copolymer blocks. By varying temperature and sample treatments, it was found that the ordered ribbon morphology represents the equilibrium structure at 25 °C, while the globular morphology is favored at 50 °C. The results suggest strategies to design the morphology and tune the dimensions of aqueous block copolymer–bile salt aggregates.

1. Introduction

Complexes of hydrophilic neutral-ionic block copolymers and oppositely charged polymers or surfactants have been extensively explored in the last few decades. In aqueous dispersions, these complexes are typically organized as core–shell nanoparticles, with a concentrated core composed of the charged block of the copolymer electrostatically complexed with the oppositely charged species, and a shell composed of the neutral hydrophilic block.[1] These co-assembled structures are often called complex coacervate core micelles (C3Ms).[2,3]

Even though the most abundant C3M systems reported consist of core–shell spheres, other morphologies can appear depending on the molecular structure of the components.[4,5] It is well known that the block length ratio of the copolymer has a determining effect on the C3Ms shape. Relatively long neutral hydrophilic blocks generally lead to the formation of spheres, whereas shorter shell-forming blocks often give rise to lower-curvature aggregates such as elongated micelles or vesicles.[6–8] Additionally, not only the morphology, but also the size, internal structure and colloidal stability of the aggregates can be sensitive to the preparation protocol and factors such as concentration, ionic strength, and temperature.[9–13] When surfactant ions are used as complexing agents, surfactant liquid crystalline structures may form in the core, giving rise to various angular particle shapes that reflect the underlying core structure.[4,12,14–17] We note, however, that also for these systems, core–shell spheres with disordered cores typically form as a result of conventional preparation protocols where solutions of the respective components are mixed. We will return to this point below.

Although not extensively explored, the use of biosurfactants such as bile salts can confer unique characteristics to

[a] *Division of Physical Chemistry, Department of Chemistry, Lund University, P.O. Box 124, SE-22100 Lund, Sweden. E-mail: karin.schillen@fkem1.lu.se*
[b] *Institute of Chemistry, University of Campinas (UNICAMP), P.O. Box 6154, 13083-970, Campinas, São Paulo, Brazil. E-mail: wloh@unicamp.br*
[c] *Department of Chemistry, Sapienza University of Rome, P.O. Box 34-Roma 62, Piazzale A. Moro 5, 00185 Roma, Italy*

† Electronic supplementary information (ESI) available. See DOI: https://doi.org/10.1039/d5sm00097a

‡ Present address: Physical and Chemical Analysis Center at Suzhou Institute for Advanced Research, University of Science and Technology of China, Suzhou 215123, People's Republic of China.

oppositely charged polymer–surfactant systems. Unlike conventional surfactants with a single hydrophilic head and a hydrophobic tail, bile salts display a rigid chiral steroidal skeleton with a complex distribution of hydrophobic and hydrophilic regions.[18] Due to the complexity of their structure, the aggregation of the bile salts often follows a stepwise process in a broad concentration interval, generating aggregate morphologies that cannot be rationalized by the geometric rules of conventional surfactant packing parameters.[19,20]

Due to their special self-assembly behavior as described above, bile salts and their derivatives are also capable of forming intriguing structures when complexed with cationic polymers or multivalent cations,[21,22] and similar structures have recently been found in C3Ms containing bile salts in their cores.[21,23] Thus, Du *et al.*[21] demonstrated that the complexation between the anionic bile salt sodium deoxycholate (NaDC), and cationic block copolymers with a neutral hydrophilic block of either poly(*N*-isopropylacrylamide) (PNIPAM) or poly(ethylene glycol) (MPEG) and a ionic block of poly(3-acrylamidopropyl)trimethylammonium (PAMPTMA(+)) (PNIPAM$_m$-*block*-PAMPTMA(+)$_{30}$ (m = 65 or 48) or MPEG$_{45}$-*block*-PAMPTMA(+)$_{21}$) promoted the arrangement of DC helices into hexagonally packed bundles and toroids. Cryogenic transmission electron microscopy (cryo-TEM) and cryogenic electron tomography (cryo-ET) analysis provided crucial structural information, enabling the development of a model to describe these assemblies: the DC helices are wrapped together in ordered hexagonally packed bundles by the cationic block of the copolymer while the neutral hydrophilic block composes the shell, providing colloidal stability to the assemblies.

In an earlier study, where a block copolymer with a longer PNIPAM block was used (PNIPAM$_{120}$-*b*-PAMPTMA(+)$_{30}$) in mixtures with NaDC, globular particles with disordered cores were obtained in addition to the internally structured bundles.[23] If the bile salt was chemically modified, only supramolecular twisted ribbons were obtained.[24] Those same systems were also explored by varying the temperature.[24,25] Due to the presence of the thermoresponsive block of PNIPAM, which displays a lower critical solution temperature (LCST) typically around 32 °C, it was observed that the complexes can display aggregation or a morphological transformation upon heating.

The previous studies highlight the versatility of block copolymer–bile salt complexes in forming diverse supramolecular morphologies. However, the factors governing the formation and stability (kinetic or thermodynamic) of each possible morphology, as well as their dimensions, remain to be understood. In the present contribution we therefore explore the supramolecular structures formed by the complexation between DC and the neutral–cationic block copolymer poly(ethylene oxide)$_{114}$-*block*-poly(2-(trimethylammonium)ethyl methacrylate)$_{95}$ (PEO$_{114}$-*b*-PTMAEMA(+)$_{95}$). Considering that the previous studies exclusively used PAMPTMA(+) as the positively charged block we sought in this study to analyze, by using a copolymer with a PTMAEMA(+) block, if the formation of DC helices and bundles of such helices in aggregates with the block copolymer critically depends on the detailed chemistry of the cationic block. Furthermore, the use of PEO as the neutral hydrophilic block allows us to explore the influence of higher temperatures on the assemblies without compromising their colloidal stability in aqueous media. The LCST of the PEO homopolymer in water is above 100 °C.[26–28] Lastly, here we use a neutral–cationic diblock copolymer where both blocks are longer than in the block copolymer–NaDC mixtures studied previously. This could play an important role for the resulting morphology and internal structure of the co-assemblies.

Dynamic light scattering (DLS), small-angle X-ray scattering (SAXS), cryo-TEM, and proton NMR techniques are employed to elucidate the morphology, size and structure of the complexes obtained. Importantly, we also employ different protocols to prepare and treat the complexes, to establish what may be their equilibrium morphology under various conditions. Our main focus is on conditions where the electrostatic attraction between the cationic block and the bile salt are at a maximum, that is, a stoichiometric charge ratio and no added salt. Occasional comparisons are made using samples with a twofold excess of bile salt.

2. Experimental

2.1 Materials

Poly(ethylene oxide)-*block*-poly(2-(dimethylamino)ethyl methacrylate) (PEO$_{114}$-*b*-PDMAEMA$_{95}$) block copolymer (M_n = 20 000 g mol^{-1}, M_w/M_n = 1.4) was purchased from Polymer Source. Inc. (Quebec, Canada). The contour lengths of the two blocks are estimated to 24 nm for PDMAEMA$_{95}$ and 41 nm for PEO$_{114}$ (see below). Prior to use, the copolymer was reacted with methyl iodide, following the procedure described by Scandalis *et al.*,[29] to promote the complete quaternization of the amine groups of the PDMAEMA block, resulting in the block copolymer poly(ethylene oxide)-*block*-poly(2-(trimethylammonium)ethyl methacrylate iodide) (PEO$_{114}$-*b*-PTMAEMAI$_{95}$) (M_n = 33 484 g mol^{-1}). The complete quaternization of the copolymer was confirmed by ^{1}H NMR measurement, as shown in Fig. S1, ESI.† Sodium deoxycholate (NaDC, assay ≥99%), deoxycholic acid (HDC, assay ≥99%), sodium cholate (NaC, assay ≥99%), and sodium iodide (NaI, assay ≥99.5%) were purchased from Sigma Aldrich and used as received. AmberTec™ UP550 OH anion exchange resin was obtained from Sigma Aldrich and used as received. Water used for the sample preparation was purified using a Milli-Q system (Millipore Corporation, Bedford, MA, U.S.).

2.2 Sample preparation

2.2.1 Direct mixing protocol. Aqueous dispersions of PEO$_{114}$-*b*-PTMAEMAI$_{95}$ and NaDC complexes were conventionally prepared at room temperature, by weighing stock solutions of the pure components, which were lyophilized before to minimize the water content, at desired molar charge ratios of negatively charged DC ions to positively charged amine groups of the copolymer (CR = n_{DC}/n_{TMAEMA}, where n_{DC} is the number of moles of bile salt and n_{TMAEMA} is the number of moles of positive charge and was estimated using molar mass of the block copolymer and the number of PTMAEMA block repetitions (= 95 units)). For this purpose, an appropriate mass of a

2.00 wt% NaDC stock solution was added to a 1.00 wt% PEO_{114}-*b*-$PTMAEMAI_{95}$ solution to achieve the desired charge ratio. Water was then added to adjust the final copolymer concentration to 0.50 wt% = 0.15 mM (from here on 0.5 wt%). Afterwards, the samples were gently stirred for a few minutes. Dispersions of PEO_{114}-*b*-$PTMAEMAI_{95}$ and NaC were prepared following the same procedure. For the SAXS measurements, the dispersions were used as prepared, *i.e.*, at 0.50 wt% of copolymer. The dispersions were diluted to a copolymer concentration of 0.050 wt% (from here on 0.05 wt%) for the DLS and electrophoretic mobility measurements, or to 0.10 wt% (from here on 0.1 wt%) for the cryo-TEM measurements.

Collectively, the dispersions prepared by this preparation protocol are referred to in this paper as PEODC (CR = *x*), where PEO refers to the PEO_{114}-*b*-$PTMAEMA(+)_{95}$ block copolymer, DC refers to deoxycholate, and CR denotes the negative-to-positive charge ratio of the complex as defined above.

2.2.2 Complex salt protocol. In addition to the block copolymer–bile salt complexes, samples prepared by the direct mixing protocol contain simple sodium and iodide ions originating from the salts used in the stock solutions. Using the following protocol, a charge-stoichiometric complex free of these simple ions was prepared. The iodide ions of the PEO_{114}-*b*-$PTMAEMAI_{95}$ block copolymer were substituted by hydroxide ions in an anion exchange resin (AmberTec™ UP550 OH anion exchange resin), following the procedure described by Svensson *et al.*[30] After the anion exchange step, aliquots of the resulting alkaline solution were titrated with a standard 0.10 mol L^{-1} (from here on 0.1 mol L^{-1}) solution of HCl in order to determine the final concentration of the hydroxide form of the copolymer. Immediately after, a stoichiometric amount of deoxycholic acid was added to the copolymer solution, rendering a dispersion of complex salt with 1 : 1 stoichiometry of charges at a final pH of 7.4. The mixture was left to react under magnetic stirring for several hours to guarantee complete homogeneity. Then, the dispersion was freeze-dried, and the complex salt was isolated as a white powder. During the ion exchange step, the quaternary amine group of PTMAEMA(+) block inevitably undergoes a Hoffman elimination reaction under alkaline conditions, generating trimethylamine and poly(vinyl methacrylate) chains as subproducts, as confirmed by ^{1}H NMR (Fig. S2, ESI†). From the pH titration curves of the alkaline copolymer solution after removal from the anion exchange resin, the second inflection point corresponding to the weak base trimethylamine indicated a 5 mol% content of Hoffman elimination products. However, since this reaction progresses over time, the extent may be higher in the complex salt, due to the delay between the titration and the addition and complete dissolution of deoxycholic acid to neutralize the copolymer solution.

The samples to be investigated were prepared by dispersing appropriate amounts of complex salt in pure water under vigorous magnetic stirring. Dispersions obtained by employing this preparation protocol will be referred to as PEODC (CS), where the terms PEO and DC are defined above, and CS refers to the complex salt protocol employed.

2.3 Methods of characterization

2.3.1 ^{1}H NMR. ^{1}H NMR spectra were obtained at the NMR center of Lund University (Lund, Sweden) and, for a few samples, at the NMR lab of Institute of Chemistry, University of Campinas (Unicamp, Campinas, Brazil), in both cases using a 500 MHz Bruker Avance spectrometer (Billerica, MA, USA) for the dispersions as well as for the solutions of the individual components (bile salt and block copolymer). All measurements were performed at 25 °C applying a delay of 3 s and a number of scans of 64.

2.3.2 DLS. DLS measurements were carried out on an ALV/DLS/SLS-5022F, CGF-8F-based compact goniometer system (ALVGmbH, Langen, Germany), equipped with a 22 mW He–Ne laser operating at a wavelength of λ = 632.8 nm, of which the intensity is varied using an automatic attenuator. The detection system comprises a near-monomodal optical fiber, and two avalanche photodiodes positioned in a pseudo-cross geometry. The comprehensive description of the instrument is found in ref. 31 with the exception that a Glan-Thomson polarizer was put in front of the detector unit to ensure vertical-vertical polarization geometry. Prior to the experiments, the block copolymer–bile salt dispersions were filtered through 0.45 μm-Millex-HV syringe filters from Millipore (now Merck Millipore) into clean cylindrical light scattering cells of borosilicate with an outer diameter of 10 mm. The light scattering cell was immersed in the vat (cylindrical quartz container) filled with *cis*-decahydronaphthalene (or decaline) as a refractive index-matching liquid. The DLS measurements were performed at different scattering angles (θ), typically in the range of 30–140° and at a constant temperature of 25.00 °C, which was controlled to ±0.01 °C by a F32 Julabo heating circulator. The analysis of the DLS data was performed directly on the normalized experimentally measured pseudo-cross time correlation function of the scattered intensity ($g^{(2)}(t) - 1$, where t is the lag time) using the regularized inverse Laplace transform (RILT) algorithm provided in the ALV software: $g^{(2)}(t) = 1 + \beta\left|\int_0^\infty A(\tau)\exp(-t/\tau)\mathrm{d}\tau\right|^2$, where τ is the relaxation time and $\beta(\leq 1)$ takes into account deviations from ideal correlation. The obtained relaxation time distributions are presented in an equal area representation as $\tau A(\tau)$ *versus* log (τ/μs). Furthermore, the apparent diffusion coefficient D_{app} of the scattering particles undergoing translational motion corresponds to the mutual diffusion coefficient in the low q regime and at finite concentrations and is given by: $D_{app} = \lim_{q\to 0}(\Gamma/q^2)$, where Γ is the relaxation frequency ($\Gamma \equiv \tau^{-1}$) and q is the magnitude of the scattering vector defined as $q = 4\pi n\sin(\theta/2)/\lambda$, where n is the refractive index of the solvent (here water). Here, in the case of the globular complexes, the measured relaxation rates were linearly dependent upon q^2 through the origin thus confirming that the intensity correlation function is associated with a translational diffusion process. The DLS measurements on the globular complexes at 25 and 50 °C were thereafter only performed at θ = 90°. The *Z*-averaged apparent hydrodynamic radius ($R_{H,app}$) of the globular complexes was calculated using the Stokes–Einstein equation: $R_{H,app} = kT/6\pi\eta_0 D_{app}$ in which k is the Boltzmann constant and η_0 is the viscosity of the solvent (here water) at the absolute temperature T.

Temperature dependent DLS measurements were performed using a Zetasizer Nano ZS instrument (Malvern Panalytical, Malvern, U.K.) equipped with a 4 mW He–Ne laser source (λ = 632.8 nm) and with a backscattering geometry at a scattering angle of θ = 173°. Samples were placed in square glass cuvettes and measured at 25 and 50 °C. The temperature was controlled by using the Peltier-thermostatted sample holder of the instrument (accuracy: ±0.1 °C). The obtained time autocorrelation functions of the scattered intensity were evaluated by the non-linear least square procedure provided by the instrument software. The latter analysis expresses the results as apparent hydrodynamic radii distributions and the quoted $R_{H,app}$ values are obtained from the main mode in the distributions.

2.3.3 Electrophoretic mobility. Electrophoretic mobility measurements of the dispersions were performed at θ = 13°, using the Zetasizer Nano ZS instrument described in Section 2.3.2. The samples were placed in disposable folded capillary cells, DTS1070 (Malvern Instruments Ltd, Worcestershire, UK) and measured at 25 °C.

2.3.4 SAXS. Small-angle X-ray scattering measurements were performed using the laboratory-based SAXSLab Ganesha 300XL instrument (SAXSLAB ApS (Xenocs), Skovlunde, Denmark) at the Division of Physical Chemistry, Lund University (Lund, Sweden). This apparatus is equipped with an X-ray source producing a photon beam with a wavelength of 1.54 Å (Cu Kα). The scattering patterns were recorded with a two-dimensional (2D) 300 K Pilatus detector (Dectris, Baden, Switzerland). Measurements were performed at a temperature of 25 °C, which was controlled by an external recirculating water bath (Julabo, Seelbach, Germany). Samples were analyzed in 1.5 mm diameter quartz glass capillaries at two different sample-detector distances covering a q-range from approximately 0.05 to 7.5 nm^{-1} (where q is equal to $q = 4\tau \sin(\theta/2)/\lambda$). The measured intensities were corrected using background scattering and sample transmission. Data were brought to absolute scale by using the absolute scattering intensity of water at 20 °C. Complementary SAXS and WAXS experiments were conducted at the Institute of Chemistry, University of Campinas (UNICAMP, Campinas, Brazil), using the laboratory SAXSPoint 5.0 equipment (Anton Paar, Graz, Austria). The wavelength of the radiation was 1.54 Å (Cu Kα). Liquid samples were loaded into 1.5 mm quartz capillaries, while gel-like samples were mounted between two mica foils. Experiments were performed at two sample-to-detector distances, covering the q-range of 7.0 to 28 nm^{-1} for WAXS measurements and 0.09 to 5 nm^{-1} for SAXS measurements. Background subtraction was performed by subtracting a water-filled capillary measurement from the liquid sample data, and a measurement of two mica foils was subtracted from the gel samples. The experimental data were fitted by Indirect Fourier Transform (IFT) analysis by using the WIFT program,[32] to obtain the pair distance distribution functions.

2.3.5 Cryo-TEM. Cryo-TEM experiments were carried out on a JEM-2200FS transmission electron microscope (JEOL) at the National Center for High Resolution Electron Microscopy (nCHREM) at Lund University. The microscope is equipped with a field-emission electron source, a cryo pole piece in the objective lens and an in-column energy filter (omega filter). Zero-loss images were recorded at an acceleration voltage of 200 kV on a bottom-mounted TemCam-F416 camera (TVIPS) using SerialEM under low-dose conditions. Specimens were prepared using an automatic plunge freezer system (Leica Em GP) under controlled temperature and relative humidity. Additional cryo-TEM experiments were carried out at the Brazilian Nanotechnology National Laboratory (LNNano, CNPEM, Campinas, Brazil) using a JEM1400Plus (Jeol, Japan) transmission electron microscope operating at 120 kV and equipped with a OneView CMOS 4k × 4k camera (GATAN, USA) for digital image acquisition. Copper grids with a Lacey-type carbon film (#01895-F, Ted Pella, USA) were used for sample deposition. The grids were treated with a load of 25 mA for 50 s in EasiGlow (I) equipment (TedPella, USA). These grids were then transferred to the Vitrobot IV sample vitrification robot (Thermo, USA). A 3 μL volume of sample was applied to each grid, and the excess sample was drained by a subsequent blotting process. The grids were then plunged into liquid ethane for rapid vitrification of the sample. After this step, the grids were kept in liquid nitrogen until insertion into the microscope.

3. Results and discussion

3.1 Samples obtained after direct mixing

3.1.1 Mixtures of core–shell aggregates: ribbons and globules. The protocol for direct mixing (see Section 2.2.1 in Sample preparation) is the same as that used in previous studies of NaDC complexed with other neutral-ionic diblock copolymers.[21,23] The cryo-TEM images in Fig. 1 show PEODC samples at CR = 1 and CR = 2, denoted PEODC (CR = 1) and PEODC (CR = 2), respectively. Both display the coexistence of globular particles and striped supramolecular ribbon-like structures.

The latter are similar in appearance as the ''bundle'' or ''tape-like'' structures found in the PNIPAM$_m$-*b*-PAMPTMA(+)$_{20}$/NaDC[21] (m = 65 or 48) and PNIPAM$_{120}$-*b*-PAMPTMA(+)$_{30}$/NaDC[23] systems. The globular particles appearing in Fig. 1 present disordered cores and are similar to those previously reported for complexes formed by PNIPAM$_{120}$-*b*-PAMPTMA(+)$_{30}$ copolymer and NaDC.[23] In the globular particles, the core is composed of anionic deoxycholate micelles complexed with cationic PTMAEMA(+) blocks, while the shell is composed by the neutral hydrophilic PEO blocks, which provide steric stability to the assemblies against further aggregation. The shell is invisible in the cryo-TEM images due to low electronic density contrast. The average core radius (R_c) determined from the images of the globular particles is 32 ± 8 nm and 30 ± 8 nm for CR = 1 and CR = 2, respectively (see size distribution in Fig. S3, ESI†). This insignificant variation in core size indicates that the excess bile salt added does not enter the core of the globules to a significant extent. The apparent hydrodynamic radii obtained from DLS measurements at the scattering angle 90° were also determined using RILT analysis (see Section 2.3.2 in Methods

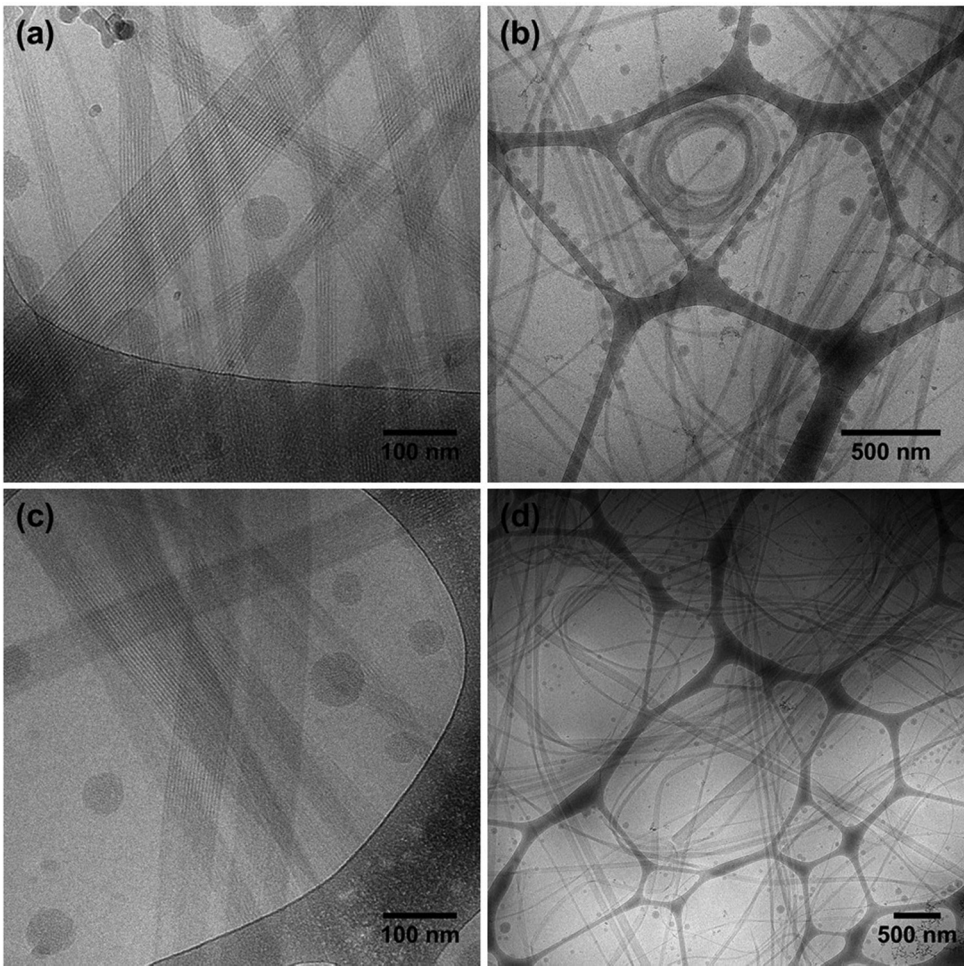

Fig. 1 Cryo-TEM images of the PEODC dispersions at CR = 1 (a), (b) and CR = 2 (c), (d) at 0.1 wt% of copolymer.

of characterization), again giving very similar values of $R_{H,app}$ = 60 nm for CR = 1 and $R_{H,app}$ = 57 nm for CR = 2. The electrophoretic mobility values were $\mu = 0.7 \times 10^{-8}$ m^2 s^{-1} V^{-1} for CR = 1 and -0.2×10^{-8} m^2 s^{-1} V^{-1} for CR = 2.

Regarding the ribbon-like structures observed in Fig. 1, it is possible to discern darker stripes within the ribbons with a periodic average distance of 5.0 nm (see Fig. S4, ESI†) for both CR = 1 and CR = 2 samples. The ribbons exhibit a distribution of widths, averaging 44 ± 21 nm for CR = 1 and 54 ± 34 nm for CR = 2 (Fig. S5, ESI†), indicating a slight dependence on the charge ratio. The first model to describe these striped structures, proposed in ref. 23, was later revised in ref. 21, identifying them as supramolecular DC helices condensed into hexagonally ordered bundles by the association with the cationic blocks of several copolymers chains. The periodic distance of 5.0 nm between the stripes is interpreted as the inter-plane distance within the structure and the value obtained is close to what is observed in the PNIPAM$_m$-*b*-PAMPTMA(+)$_n$/NaDC systems[21,23] and it also consistent with that of the hexagonal liquid-crystalline phase in the NaDC/water system at high concentration.[33] As in the globular particles, the PEO block protrudes out from the ribbons, providing colloidal stability in aqueous media.

The locations of the two polymer blocks and the DC molecules in the aggregates were confirmed by ^{1}H NMR analyses of the dispersions (Fig. 2). While solutions of the pure block copolymer and pure bile salt show several sharp peaks (Fig. 2(a) and (b)), most of these peaks are broadened beyond detection in the spectra of the dispersions at CR = 1 and CR = 2. The latter spectra show only three peaks: from the block copolymer, a sharp PEO peak and a broader peak corresponding to the *N*-methyl protons of the cationic block, and from the bile salt a non-resolved, very broad peak in the region 0–2.5 ppm. Due to the preserved mobility of the PEO chains protruding from the aggregate surfaces, their signal remains narrow and intense in the ^{1}H NMR spectrum (analogous effects were found in the PNIPAM$_{48}$-*b*-PAMPTMA(+)$_{20}$/NaDC system).[21] In the cationic block, the *N*-methyl groups of the (trimethylammonium)ethyl side chains remain relatively mobile, while the signals from the other protons have disappeared. As expected, the bile salt peak increases in intensity for the CR = 2 sample, which contains excess NaDC. However, no high-resolution signal is seen from the excess bile salt, indicating a rapid exchange (on the NMR timescale) of the excess DC anion in solution with DC anions residing in the aggregates.

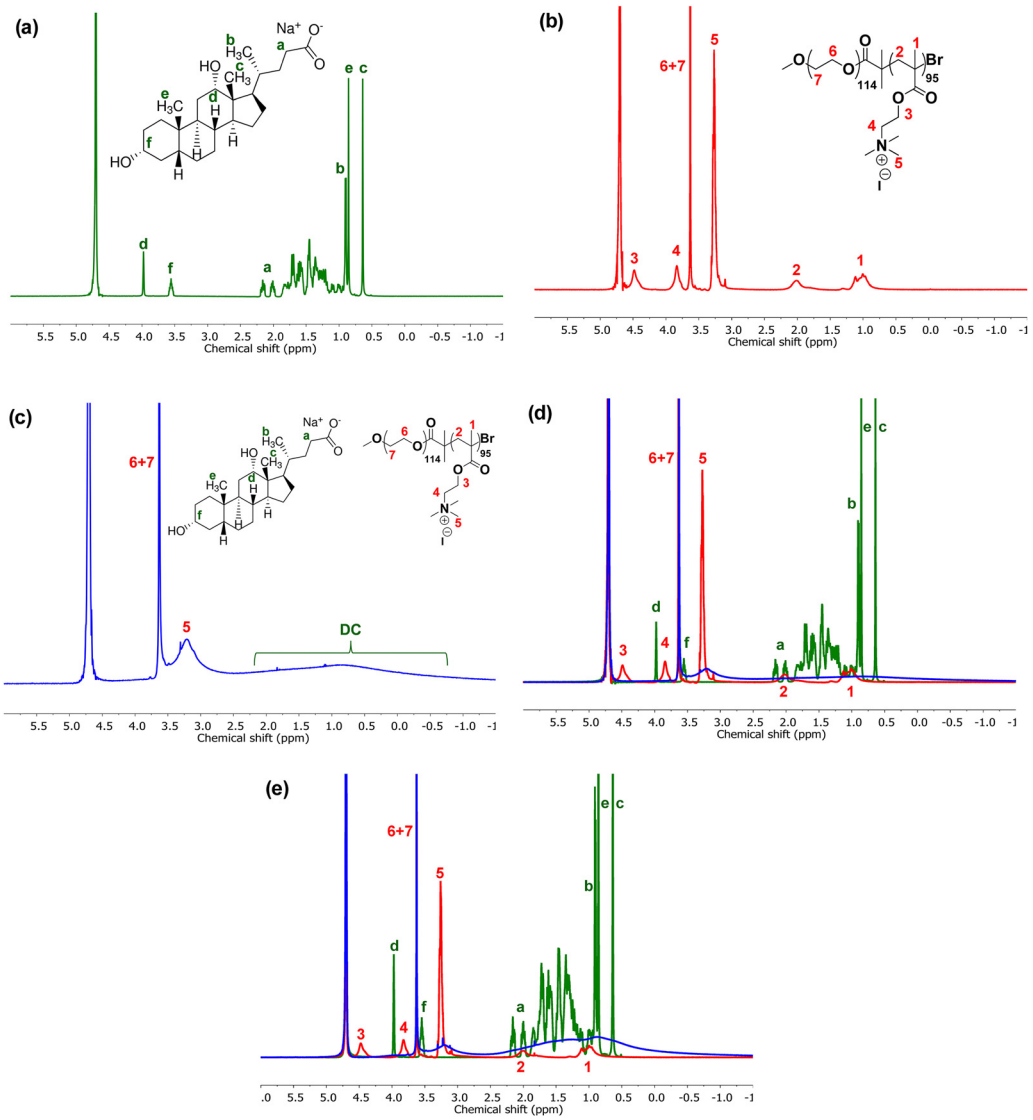

Fig. 2 ^{1}H NMR spectra in D_2O of the pure components: 14.18 mM of NaDC (a), 0.5 wt% of PEO_{114}-*b*-PTMAEMAI$_{95}$ (b), and of the dispersion of PEODC (CR = 1) (c) containing 14.18 mM of NaDC dispersed at 0.5 wt% of copolymer. (d) Superimposed spectra from panels a, b, and c. (e) ^{1}H NMR spectra of the PEODC (CR = 2) dispersion, containing 28.36 mM of NaDC and 0.5 w% of copolymer, together with the spectra from NaDC and PEO_{114}-*b*-PTMAEMAI$_{95}$ pure solutions with the same concentrations as in the dispersion. For comparison of the peak intensities, all the superimposed spectra are on the same scale in (d) and (e). NaDC peaks were assigned according to ref. 34.

For a quantitative evaluation of the intensities of the visible signals, the latter signals were integrated and compared to the corresponding signals from the pure reference solutions at the same concentration. Due to the presence of broad and overlapping peaks, the spectra of the PEODC complexes were deconvoluted using Lorentzian fitting to enable peak integration. Table 1 shows the relative peak area ratios for the complexes. The PEO peak displays an area unchanged compared to that of the pure copolymer solution, confirming that the PEO chains reside fully exposed on the aggregate surfaces, where they are highly mobile. By contrast, the signals from DC ions and PTMAEMA(+) chains, which are electrostatically complexed in the ribbons' skeleton or the particles cores, are attenuated. The apparent relative intensity of the DC signal is higher at CR = 2 than at CR = 1, which is to be expected; the excess free DC ions in solution should contribute at full strength to the observed intensity. Note that, also under conditions of charge stoichiometry (CR = 1), a small fraction of DC ions are dissociated from the aggregate surfaces, as indicated by the positive surface charge seen in the electrophoretic mobility measurements. By analogy with NMR results from simpler block copolymer/surfactant aggregates,[35] we conclude

Table 1 Ratio of the absolute ^{1}H NMR peak areas between the PEODC complexes and their respective pure component solutions at the same concentrations

Sample	PEO	*N*-Methyl PTMAEMA(+)	DC
PEODC (CR = 1)	0.95	0.68	0.50
PEODC (CR = 2)	1.03	0.78	0.81

that the resulting NMR peak shape and intensity are the result of a surface fraction of DC ions in rapid (on the NMR timescale) exchange with free DC ions. Both at CR = 1 and at CR = 2, the reduction in intensity could be due to DC ions residing deep into the aggregates, which do not participate in the rapid exchange.

The coexistence of globular particles and ribbons, two structures with such drastic morphological differences, turns their characterization by scattering techniques challenging. The expected scattering features of both structures, such as a globular form factor and a sharp correlation peak related to the periodic distribution of the deoxycholate helices in the ribbons were not discerned in the SAXS scattering profile of the dispersions, as can be seen from Fig. S6 (ESI†). This effect in the resulting scattering can be attributed to the polydispersity and polymorphism of the samples.

3.1.2 Physical separation between globules and ribbons. To elucidate the individual characteristic of each structure, they were physically separated through centrifugation. Centrifugation has been reported as an efficient method to separate colloidal particles of different shapes and aspect ratios.[36,37] After being submitted to centrifugation at 7000 rpm for 2 h, the PEODC (CR = 1) dispersion underwent a macroscopic phase separation, forming a blueish top phase and a concentrated gel-like bottom phase. Each phase was collected and characterized. According to the cryo-TEM images recorded from the top phase, it contained only the globular particles, with an average R_c of 25 ± 4 nm (Fig. S7, ESI†), as can be seen from Fig. 3(a).

The separation of the globular particles from the ribbons was also confirmed by SAXS, which revealed a scattering profile characteristic of globular particles (Fig. 4(a)). The SAXS data was fitted using the Indirect Fourier Transform (IFT) method.[32] The pair distance distribution function ($p(r)$) (Fig. 4(a), inset), resulting from the fit, displays a symmetric bell shape curve with a maximum distance of 72 nm. This distribution profile is characteristic of spherical particles.[10,38] The radius of gyration (R_g) calculated from the fit is 25.6 ± 0.3 nm.

A similar result was obtained by filtration of PEODC (CR = 1) sample with a 0.45 μm pore size filter. After filtration, only globular particles remained in the sample, indicating that the ribbons were retained in the filter or transformed to globules upon shearing (see cryo-TEM image in Fig. S8a, ESI†). The R_g value obtained from the IFT analysis of the SAXS curve (Fig. S8b, ESI†) was R_g = 26.7 ± 0.4 nm. These R_g values are in good agreement with the average core radius obtained by cryo-TEM (R_c = 32 ± 8 nm and 30 ± 8 nm for CR = 1 and CR = 2, respectively, Fig. S3, ESI†). In these systems, we can infer that the R_g value obtained by SAXS refers to the core radius of the particles, since the PEO chains that compose the shell are highly hydrated and do not present a sufficient electronic density contrast to be discerned from the background.

The concentrated bottom phase of the centrifuged sample was found to primarily contain the ribbon-like structures as confirmed by the presence of a first order Bragg peak at q = 1.3 nm^{-1} in the SAXS curve (Fig. 4(b)) from which a mean interplane distance, indicating the hexagonal liquid crystalline structure of the ribbons, can be calculated using $d = 2\pi/q$. The d-spacing obtained is 4.8 nm, which is in excellent agreement with that obtained in ref. 21, and in close agreement with the mean distance of 5.0 nm estimated from the cryo-TEM images (Fig. S4, ESI†). This result demonstrates that the formation and structure of the DC helices are not critically dependent on the chemistry of the cationic block, as the use of PAMPTMA(+) and PTMAEMA(+) yielded complexes with indistinguishable internal structure characteristics.

The bottom phase was redispersed in water and further analyzed by cryo-TEM confirming that, after concentration, the ribbons can be redispersed, preserving their structure, as depicted in Fig. 3(b). The ribbon-rich bottom phase was also characterized by WAXS, which revealed the presence of Bragg diffraction peaks characteristic of the helical arrangement of the deoxycholate molecules inside the ribbons (see Fig. S9a, ESI†). This result is in good agreement with the X-ray pattern

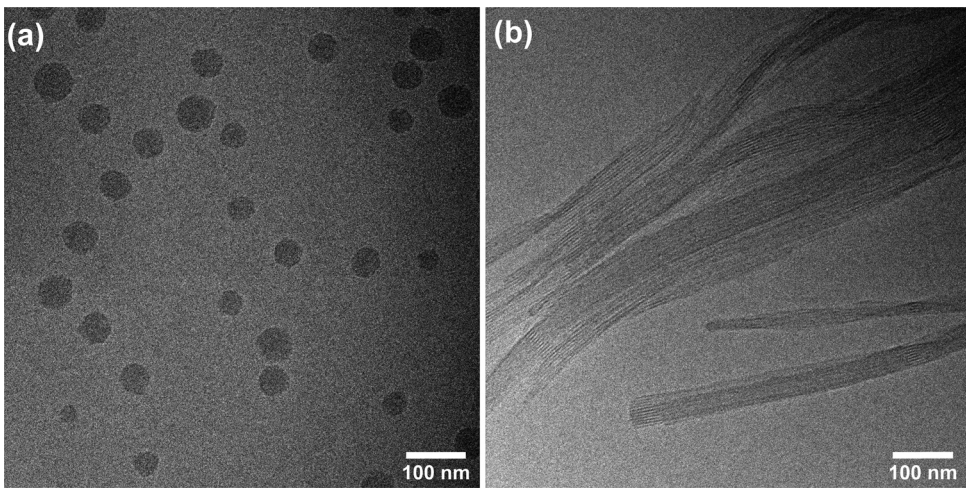

Fig. 3 Cryo-TEM images of the top phase (a) and the redispersed bottom phase (b) collected after centrifugation of a PEODC dispersion at CR = 1. The copolymer concentration was 0.1 wt%.

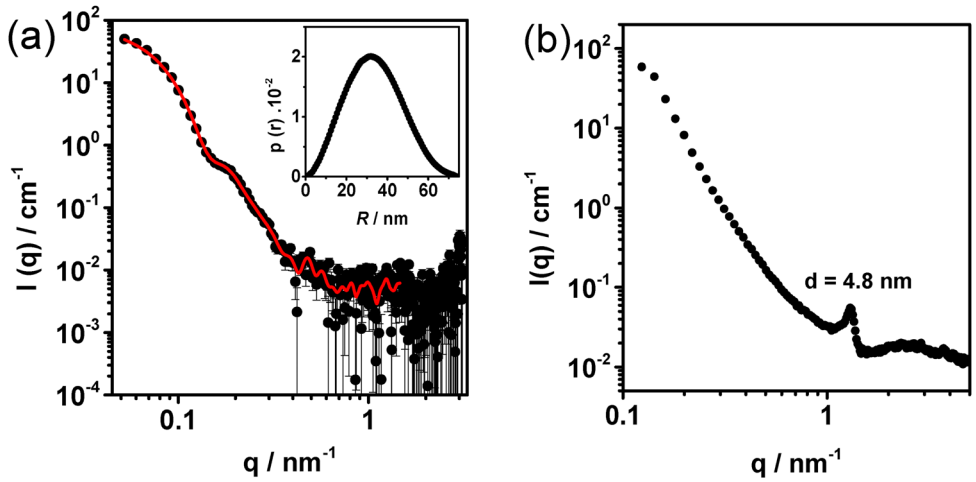

Fig. 4 SAXS patterns (black symbols) for the top phase (a) and bottom phase (b) obtained after centrifugation of a PEODC dispersion at CR = 1 with a copolymer concentration of 0.5 wt%. Panel (a) also displays the curve fitting (red line) obtained by IFT analysis and the corresponding pair distance distribution function ($p(r)$) (inset).

obtained for dry helical fibers of pure NaDC[39,40] and the results previously reported for similar block copolymer/DC systems.[21]

Furthermore, as can be seen in the cryo-TEM images, especially in Fig. 1, the ribbons are relatively transparent, so that it is possible to observe one ribbon through the other in the microscopy grid. Additionally, the images in Fig. 1(b) and (d) show that the PEODC ribbons are quite flexible, in such a way that they can twist, fold and form rolled up assemblies. Overall, these features indicate that the ribbons are composed of only a few layers of long bile salt helices. No thicker bundles or toroidal structures, as reported by Du *et al.*[21] in some systems, were observed in the present study.

3.1.3 Globules change to ribbons with time. To investigate if the globular particles collected from the centrifuged sample could eventually evolve to ribbons, they were analyzed 15 days after centrifugation by cryo-TEM. Fig. 5(a) shows that ribbon-like structures had indeed formed in the sample.

Comparing the image in Fig. 5(a) with that in Fig. 3(a) (recorded the same day as the centrifugation process), it is clear that globular particles evolve, given sufficient time, into the ribbon morphology. The same behavior was observed for the dispersion analyzed one day after filtration (Fig. 5(b)), where short ribbons were already detected. Note, however, that both Fig. 5(a) and (b) still show the presence of globular particles coexisting with the formed ribbons; the transition is not complete. Nevertheless, the fact that the globular particles transition to ribbons over time at room temperature strongly suggests that the ribbon-like structure represents a lower free energy state for the PEODC complexes.

3.2 Changing the preparation protocol

3.2.1 Complex salt samples. It is well known that out-of-equilibrium polyion–surfactant ion complexes are highly

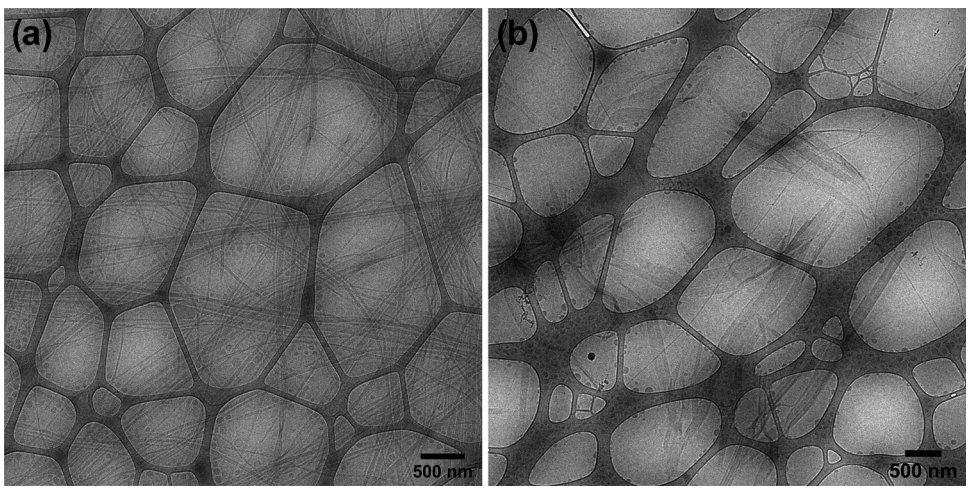

Fig. 5 (a) Cryo-TEM image of the collected top phase of PEODC (CR = 1) dispersion 15 days after centrifugation. (b) Cryo-TEM image obtained from a PEODC (CR = 1) dispersion recorded the day after filtration with a 0.45 μm pore size filter. Both images show ribbons coexisting with globular particles. The copolymer concentration was 0.1 wt%.

sensitive to the preparation protocol.[12,16,41–45] As a radically different method of producing PEODC complexes, the complex salt protocol was used.[30] The protocol involves ion exchange, acid–base titration, freeze-drying and redispersion, resulting in a dispersion of a charge-stoichiometric complex free of simple counterions (see description in Section 2.2.2 in Sample preparation). The complex salt dispersion displayed a significantly more turbid appearance than dispersions obtained by the direct mixing protocol. Cryo-TEM images of the PEODC complex salt dispersion (PEODC (CS)) (Fig. 6(a)) revealed that only ribbon-like aggregates were formed, and globular particles were not detected.

This result suggests that, in the complex salt dispersion, the components are involved exclusively in ribbons. The larger proportion of ribbons was also reflected in the appearance of a correlation peak in the SAXS curve referring to the periodicity of the NaDC helices in the ribbons (inter-plane distance), as depicted in Fig. 6(c). This peak was not visible in the direct mixing sample at the same copolymer concentration (see Fig. S6, ESI†). An analysis of the cryo-TEM images revealed that the ribbons in the PEODC (CS) sample had a larger average width compared to those in the PEODC (CR = 1) sample, with values of 65 ± 24 nm (Fig. S10, ESI†) and 44 ± 21 nm (Fig. S5a, ESI†), respectively. However, the ribbons retained the same helical arrangement of the deoxycholate molecules, as confirmed by the Bragg diffraction peaks observed in the WAXS data presented in Fig. S9b (ESI†).

To check whether the presence of counterions *per se* plays a critical role in the formation of globular particles, a sample of PEODC complex salt was dispersed in NaI solution, yielding a dispersion with the same composition as the direct mixing sample. Analyses of the former sample using cryo-TEM and

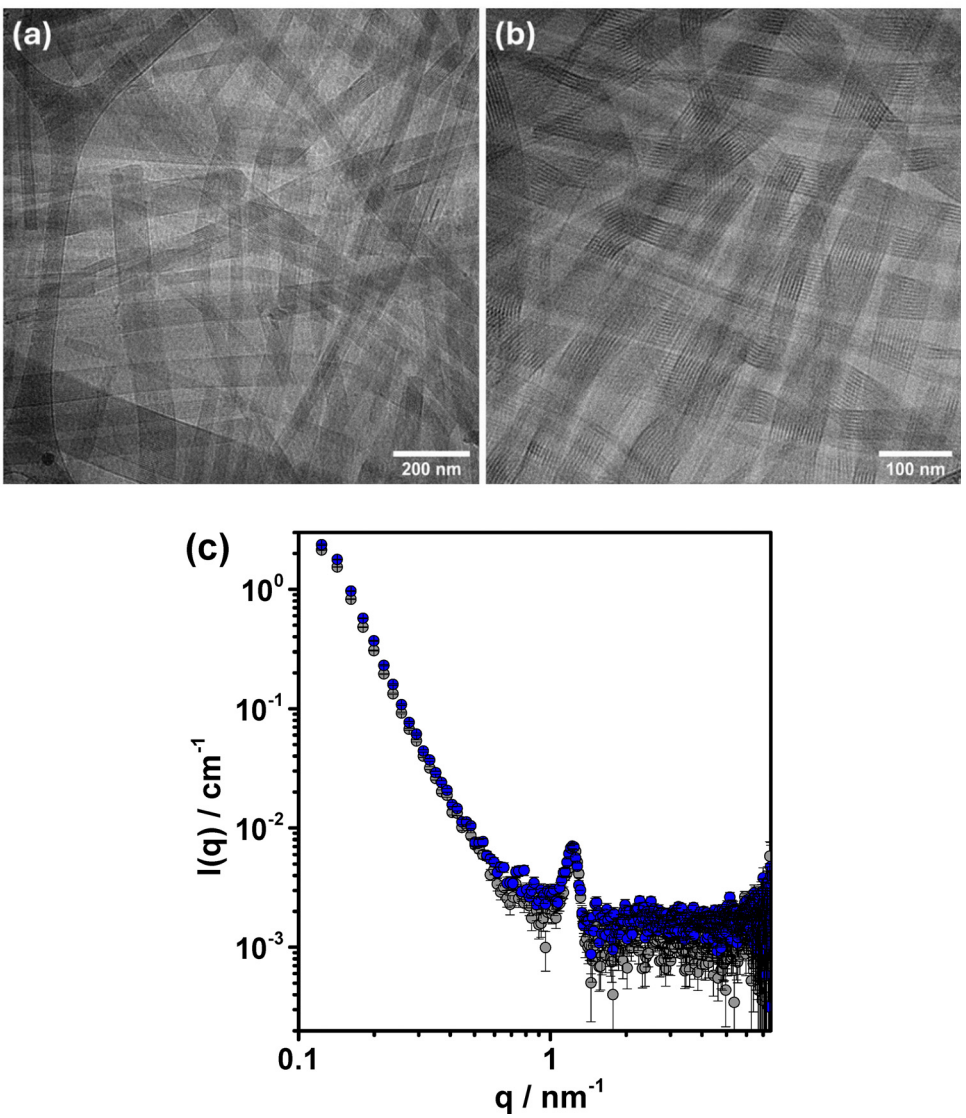

Fig. 6 Cryo-TEM images of PEODC complex salt dispersions at 0.1 wt% of copolymer without (a) and with the addition of NaI (b) at an equivalent amount to that in the PEODC (CR = 1) prepared by direct mixing protocol. (c) SAXS curves for the same dispersions at 0.5 wt% of copolymer. Gray symbols: pure PEODC (CS) dispersion; blue symbols: PEODC (CS) dispersion + NaI.

SAXS (see Fig. 6(b) and (c)) showed no presence of globular particles. The only structural effect detected was that the ribbons were narrower (W = 53 ± 24 nm) in the presence of NaI, compared to those in the salt-free PEODC complex salt (W = 65 ± 24 nm) (see Fig. S10, ESI†). This result suggests that the presence of small amounts of simple salt is not a critical factor for the formation of globules.

As the PEODC (CS) sample only contained ribbon-like aggregates, their ^{1}H NMR peak intensities were analyzed and compared with PEODC (CR = 1), which contained both ribbons and globules, and the PEODC (CR = 1) top phase sample, which contained essentially only globules. As shown in Table S1 (ESI†), the relative DC integrals reveal that the DC signal intensity is more attenuated for the PEODC (CS) sample compared to the other samples, especially compared to the PEODC (CR = 1) top phase sample, indicating that intensity loss is significantly larger for ribbon-like aggregates than for globules. This aligns with the expected greater mobility of DC anions in the disordered core of the globules compared to the tightly packed DC anions in the helical structures within the ribbons. A smaller fraction of DC ions in the core should also be involved in rapid molecular exchange with free DC ions in the bulk when the DC molecules are assembled into crystalline helical rods.

3.2.2 Freeze-drying a directly mixed sample. To evaluate whether the freeze-drying process used in the complex salt preparation protocol affects the structure of assemblies formed in aqueous dispersion, a sample of PEODC (CR = 1) prepared using the direct mixing protocol was freeze-dried, and the resulting powder was redispersed in water. The SAXS curve (Fig. S11, ESI†) of the obtained dispersion revealed a correlation peak at the same q position as that observed for the bottom phase of the centrifuged sample (see Fig. 4(b)). This result suggests that redispersion of the freeze-dried PEODC (CR = 1) complex led to the formation of a larger proportion of ribbons, enabling the detection of the correlation peak in the SAXS curve.

3.2.3 Increasing the concentrations in direct mixing. Finally, we observed that changes in the concentration of the stock solutions used during the direct mixing protocol affect the size distribution and turbidity of the assemblies. As can be seen in Fig. S12 (ESI†), doubling the concentration of both copolymer and NaDC stock solutions used in the direct mixing, followed by dilution by an equal volume of water, results in a more turbid dispersion with slightly larger globular particles compared to a dispersion of the same final composition obtained from stock solutions at the standard concentrations used here. This behavior may be a consequence of the local concentration inhomogeneities developed during mixing.[43] From the differences in turbidity alone, it is difficult to estimate whether the relative proportions of globular particles and ribbons changes when higher concentrations of the stock solutions are used in the mixing protocol. However, after being subjected to centrifugation, the more turbid dispersion resulting from the latter protocol generated a larger amount of bottom phase, which may suggest that more ribbons were formed.

The above findings indicate that the formation of the ribbons is facilitated when there is a locally high concentration of bile salt and block copolymer during mixing. This effect is even more pronounced when these components are associated in powder form before dispersion in water, as is the case with the complex salt and the freeze-dried directly mixed samples.

3.3 Reversible melting of ribbons to globules

In contrast to PNIPAM, PEO is known not to undergo phase transition in water upon heating below the normal boiling point.[46,47] To evaluate the impact of temperature on the stability of the two competing structures, the PEODC (CS) sample was characterized by SAXS and DLS at 25 and 50 °C. Fig. 7(a) compares the SAXS curves of the PEODC (CS) dispersion measured at 25 °C, 50 °C and then again at 25 °C.

The scattering profile shows that, after heating to 50 °C, the correlation peak corresponding to the periodic distance

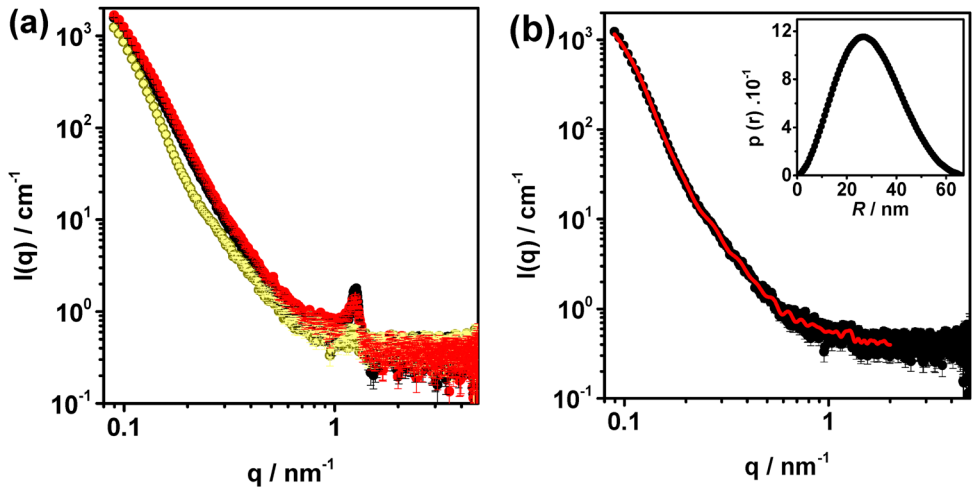

Fig. 7 (a) SAXS curves for a PEODC (CS) dispersion with a copolymer concentration of 0.5 wt% measured at different temperatures: at 25 °C (black curve); heated and equilibrated at 50 °C (yellow curve); cooled and equilibrated at 25 °C again (red curve). (b) SAXS pattern of the sample at 50 °C (same black curve as in panel a) and curve fitting (red line) obtained by IFT analysis and the corresponding pair distance distribution function ($p(r)$) (inset).

between the deoxycholate helices in the hexagonal array (interplane distance) in the ribbons disappears, indicating that the ribbons disintegrate upon heating. The increase in temperature disrupts the helical packing of the bile salt in the ribbon structure.[19,48,49] This leads to a structural rearrangement to a globular morphology, as revealed by the bell shape of the pair distance distribution function ($p(r)$) shown in Fig. 7(b) (inset), resulting from the fit of the SAXS profile at 50 °C. The R_g obtained from the fit for these globular particles was 23.1 ± 0.4 nm, in close agreement with the globules obtained by direct mixing. After the sample was cooled back to 25 °C, the ribbons gradually reformed, and the correlation peak became apparent again, evidencing the reversibility of the temperature-induced morphological transition. The melting transition was also studied and confirmed by DLS measurements (Fig. S13, ESI†).

3.4 Shape and dimensions of ribbons

From the above observations, we can conclude that the core organization of deoxycholate anions into hexagonally packed helices, and the resulting formation of ribbon-like aggregates, represent a lowering of the free energy of the PEODC aggregates compared to the disordered globules. How do we understand the shapes of the ribbon-like aggregates? The elongated structure is a natural consequence of the hexagonal packing of the helices combined with the restrictions imposed by the neutral chains of the block copolymer, the latter preventing formation of an infinite hexagonal array. For a more detailed understanding, we need to consider the lengths of the two blocks in the copolymer.

From the cryo-TEM images, we observe that the aggregates are not only elongated along the long-axis of the DC helices but also tend to lie flat on the grid displaying a width significantly greater than their thickness. The flat ribbon shape differs from the most intuitive shape expected for a rod with a 2D hexagonal internal structure, which would possess a regular hexagonal cross section with equal lengths of all sides. The deviation must ultimately be due to the repulsion between the PEO chains located on the surfaces of the aggregates. A hypothetical regular hexagonal rod, with a single cross-sectional dimension limited only by the PTMAEMA(+) contour length, would possess a significantly lower curvature than the globule with the corresponding diameter and, consequently, a stronger repulsion between the PEO chains in the shell. To decrease this repulsion, a thinner rod would be required, with a higher curvature and, also, a larger area per copolymer molecule at the surface of the core (since the volume per cationic block in the core must be conserved). However, the thinner rod would also reduce the number of stabilizing interactions per unit volume in the core. A way to make the cross-sectional area expand is to allow the aggregate to grow in one lateral dimension, into a ribbon, and we propose that this is the reason for the anisometric shape of the cross section. On the other hand, the ribbon shape results in a further decrease in curvature of the interface, compared to the hypothetical hexagonal rod. This should lead to a further reduction of the thickness of the ribbon, because of the increased repulsion between the PEO chains in the shell.

The resulting morphology is a ribbon-like aggregate with a thickness (as is clear especially from the occasional twisted ribbons found in the cryo-TEM images) much thinner than twice the contour length of the PTMAEMA(+) block. However, the length of the latter block is still important for the thickness of the ribbon, since a longer block would allow the thickness of the ribbon to increase at a preserved repulsion between the PEO chains on the surface. Conversely, a shorter neutral block would decrease the headgroup repulsion and, at a constant cationic block length, allow the ribbon to grow in thickness. This balance explains why thicker hexagonally packed bundles and toroids are obtained when copolymers with a shorter neutral hydrophilic block (PNIPAM$_m$-*b*-PAMPTMA(+)$_{20}$ (m = 65 or 48) and MPEG$_{45}$-*b*-PAMPTMA(+)$_{21}$) are complexed with NaDC.[21] In good agreement with this hypothesis, the formation of toroidal assemblies was not observed in the system containing NaDC and the block copolymer containing a long PNIPAM block with 120 repeating units.[23]

The edges of the ribbon are highly curved, which serves to decrease the average repulsion between PEO chains. This effect should influence the equilibrium width of the ribbon. However, our results clearly show that the ribbon width is at least partly determined by kinetic effects. Ribbons obtained from the complex salt preparation protocol are, on average, wider than those obtained from the direct mixing protocol (see Fig. S5 and S10, ESI†).

3.5 Understanding the globular aggregates

To further investigate the preferred aggregation behavior in the absence of bile salt helix formation, we studied a mixture of PEO$_{114}$-*b*-PTMAEMAI$_{95}$ with sodium cholate (PEOC complex), prepared by the direct mixing protocol at CR = 1. Trihydroxy bile salts, such as cholate, are known to self-assemble into smaller aggregates and are less prone to form helical arrangements.[50–52] A cryo-TEM image of the PEOC complex (Fig. 8(a)) displays only globular particles with cores lacking internal order and an average R_c = 36 ± 7 nm (Fig. S14, ESI†). These particles presented a mean $R_{H,app}$ value of 70 nm and a slight positive electrophoretic mobility value of μ = 0.96 × 10^{-8} m^2 s^{-1} V^{-1}. Similarly to the PEODC (CR = 1) globules, the globular structures of PEOC (CR = 1) were preserved at 50 °C, maintaining an $R_{H,app}$ unchanged at 70 nm after heating, as illustrated by the relaxation time distributions shown in Fig. 8(b).

In directly mixed complexes of neutral-ionic diblock copolymers with oppositely charged single-chain surfactants, the resulting assemblies are typically core–shell aggregates where the core radius is limited in at least one dimension by the length of the ionic block.[12,53,54] In PEO$_{114}$-*b*-PTMAEMA(+)$_{95}$, the contour lengths, *i.e.*, the maximum end-to-end distance in all-*trans* conformation, R_{max}, of the two blocks are estimated to 24 nm for PTMAEMA(+) and 41 nm for PEO, using $R_{max,PTMAEMA}$ = 0.252 $N_{PTMAEMA}$ (in nm)[23] and $R_{max,PEO}$ = 0.358 N_{PEO},[55,56] respectively, where N is the number of repeat units in each case. Considering the block length asymmetry of PEO$_{114}$-*b*-PTMAEMAI$_{95}$ – the neutral PEO block is almost twice as long as the PTMAEMA(+)

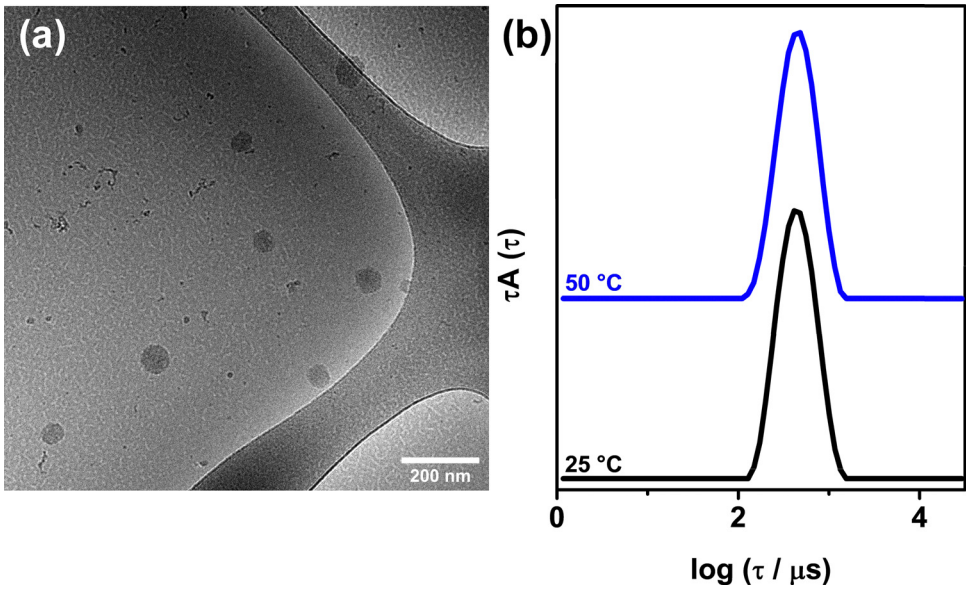

Fig. 8 (a) Cryo-TEM image of a PEO-cholate (CR = 1) aqueous dispersion at 0.1 wt% and (b) relaxation times distributions obtained by non-linear least squares fit of the intensity autocorrelation functions from DLS at 25 °C and 50 °C (both corresponding to $R_{H,app}$ = 70 nm) for the same sample diluted to 0.05 wt%. The *x*-axis is corrected for the change in absolute temperature and solvent viscosity relative to 25 °C by multiplying a correction factor of $(T/\eta_0)/(298/\eta_{298})$. The distributions were normalized to their maximum height and shifted along the *y*-axis to enhance visualization. The scattering angle was 173°.

Table 2 Values of maximum end-to-end distance (R_{max}) in all-*trans* conformation of the cationic block, average core radius (R_c) from cryo-TEM experiments at 25 °C on the globular particles in this work and in ref. 23

Samples	R_{max}/nm (cationic block)	R_c/nm (cryo-TEM)
PEODC (CR = 1)	24	32
PEODC (CR = 2)	24	30
PEOC (CR = 1)	24	36
$PNIPAM_{120}$-*b*-$PAMPTMA(+)_{30}$/NaDC CR = 1[23]	8	10

block – and the strong steric repulsion between the long PEO chains on the particles shell, high curvature aggregates, such as globules, are likely to form in the absence of core ordering, as found in the present study. Similar globular particles were also obtained in the $PNIPAM_{120}$-*b*-$PAMPTMA(+)_{30}$/NaDC system reported in ref. 23. Table 2 summarizes the measured core radii of the globular aggregates in the present work and in ref. 23, and shows that the core radius is comparable in length to R_{max} of the cationic block. Cases where the core radius exceeds this delimitation can be explained by the inevitable polydispersity of the ionic block length.[57–59] A fraction of long polyions can extend further inside the core, resulting in particles with larger average core radii. Additionally, slight deviations from a spherical shape, such as oblate and prolate shapes,[12] can also contribute to generate particles with core radii exceeding the ionic block average length.

3.6 When and why do we find metastable globules?

Our results show that globular particles represent an initial aggregation state when dilute solutions of NaDC and PEO_{114}-*b*-$PTMAEMAI_{95}$ are directly mixed, and that the globules evolve over time into ribbons or bundles. Why, then, are globules not always observed in systems where NaDC and oppositely charged block copolymers are directly mixed at charge stoichiometry? Complexes formed from shorter block copolymers, as reported in ref. 21, feature only hexagonally packed bundles and toroids; globules are not detected. Possibly, in these systems, the comparatively lower repulsion between the shorter neutral hydrophilic chains reduces the energy barrier for the transition from globules to bundles of helices. As a result, the initially formed globules rapidly evolve into bundles, rendering them undetectable. An alternative explanation is that the preferred shape of an initially formed aggregate with a disordered core is not a globule but, rather, an elongated aggregate, owing to the relatively short length of the neutral block. This already elongated shape would facilitate the rapid ordering of the core into an extended hexagonally packed ribbon.

For dispersions produced by dispersing a freeze-dried complex, DC helices likely exist already in the solid state. Accordingly, no globular intermediates were seen in the complex salt dispersions. Similarly, the liquid-crystalline core order clearly increased in a directly mixed sample after freeze-drying and redispersion (Fig. S11, ESI†). We note in passing that the initial states, before (re)dispersion, were not identical in the two freeze-dried samples. Only one combination of ions can form in the solid state on freeze-drying a complex salt, while three additional combinations are possible when freeze-drying a solution containing also the "original" simple counterions, sodium and iodide.

Metastable core–shell aggregates with disordered cores form also in situations when neutral-ionic diblock copolymers are directly mixed with common single-tail surfactants of opposite charge, and where the equilibrium surfactant ion-polyion core

features a liquid-crystalline order. Specifically, systematic studies on stoichiometric complexes between alkyltrimethylammonium surfactants and poly(acrylamide)-*block*-poly(acrylate) copolymers of a range of block lengths ($PAAm_x$-*b*-C_nTAPA_y complexes, for short) have shown that small core–shell aggregates with disordered cores result from a direct mixing protocol, whereas larger aggregates with liquid crystalline cores are formed when using the complex salt protocol.[1,12,16] The liquid crystalline structures found in the block copolymer complex salts were the same as those observed in hydrated complex salts formed by the same surfactant ions with the polyacrylate homopolymer.[17] A study of very concentrated (up to 80 wt%) mixtures of the $PAAm_x$-*b*-C_nTAPA_y complex salts in water showed that their equilibrium states were, in fact, hierarchically ordered structures, featuring one liquid crystalline order on the block copolymer length scale and another one on a much shorter surfactant length scale inside the surfactant ion-polyion domains.[60] All systems studied in ref. 60 showed a finite swelling in water, indicating that the concentrated hierarchically ordered phases represent the equilibrium states of the complexes, also in the presence of excess water.

Notably, no results obtained so far in $PAAm_x$-*b*-C_nTAPA_y systems have indicated that the small core–shell spheres formed on direct mixing eventually transform into larger aggregates with ordered surfactant domains. Thus, there are striking differences in behavior between the block copolymer–deoxycholate systems studied here and in ref. 23, on the one hand, and the previously studied $PAAm_x$-*b*-C_nTAPA_y systems: although both types of system feature (1) an initial formation of metastable core–shell globules with amorphous cores on direct mixing and (2) larger structures with ordered cores at equilibrium, aggregate growth and core ordering occurs relatively rapidly in deoxycholate based systems, whereas no such transition with time has been observed in the $PAAm_x$-*b*-C_nTAPA_y systems. From available experimental data, the origin of this interesting and practically important difference is not immediately obvious. The copolymer block lengths and length ratios do not offer any explanation. Including the results from ref. 23 we find mixtures of ribbons and globules in two NaDC-based systems featuring block copolymers that differ significantly in the block length ratio (4 and 1.7), in the length of the charged block (30 or 95 repeat units) and in the chemistries of both blocks. For comparison, the studied $PAAm_x$-*b*-C_nTAPA_y systems include the $PAAm_{133}$-*b*-$PA(-)_{49}$ block copolymer, which is comparable to $PNIPAM_{120}$-*b*-$PAMPTMA(+)_{30}$ and PEO_{114}-*b*-$PTMAEMA(+)_{95}$ regarding the block lengths, and intermediate between them regarding the length ratio.

The additional electrostatic stabilization of the dispersed particles could potentially be important for the rate of aggregate growth, but in the present study we saw little effect of changing the surface charge (CR = 2 *vs.* CR = 1; Fig. 1 and Table 2) on the aggregates obtained in directly mixed systems. Similarly, for the $PAAm_{420}$-*b*-$C_{12}TAPA_{70}$ system, Berret *et al.* saw no strong variation of the size of the (metastable) globules over a range of charge ratios around unity, where the surface charge is expected to change sign.[1]

In making the above comparisons we have tacitly assumed that aggregate growth is a necessary first step in the development of a core structure with long-range order. For $PAAm_x$-*b*-C_nTAPA_y systems, this assumption is supported by the finding that a partial ordering into a micellar cubic structure could indeed develop after direct mixing in a chemically quite similar system, PEO_{705}-*b*-$PMAA_{476}$ complexed with *N*-dodecylpyridinium cloride, but where the very long block copolymer resulted in globules with exceptionally large cores.[14]

4. Conclusions and outlook

Two radically different types of aggregate in diblock copolymer–bile salt complexes, sometimes coexisting, have been found and studied in this work: either ordered elongated ribbon-like structures, or globules with disordered cores, both featuring a concentrated core of the PTMAEMA–bile salt complex and a shell of fully hydrated PEO chains. The equilibrium structure depends on two key factors: the propensity of the bile salt to assemble into supramolecular helices, and the lengths of the two blocks of the copolymer. At room temperature, deoxycholate, which exhibits a strong tendency to pack into helices, prefers to form ribbons of hexagonally packed bile salt helices in its complexes with PEO_{114}-*b*-$PTMAEMA(+)_{95}$. Under conditions where helix formation is not favored, such as for deoxycholate at 50 °C or for cholate already at room temperature, the aggregate shape is dominated by the geometrical characteristics of the block copolymer leading, for the copolymer used here, to the formation of classical globular particles with disordered cores. When dispersions are produced at room temperature by the direct mixing of stock solutions of NaDC and PEO_{114}-*b*-$PTMAEMAI_{95}$, metastable globular aggregates are formed in addition to the ribbons, but with time, the globules disappear in favor of the ribbons.

Previous studies on complexes between NaDC and cationic–neutral block copolymers with other block lengths have demonstrated internally ordered aggregates with shapes other than ribbons, such as thicker bundles or toroids. In one case, where the block copolymer had relatively long blocks, globular particles, analogous to those found here, were also formed. It is thus quite clear that the block copolymer lengths and length ratios control, in complexes with NaDC, both the occurrence of long-lived metastable globules with disordered cores, and the shapes and dimensions of the thermodynamically preferred elongated aggregates with ordered deoxycholate helices in their cores. Collectively, the present and previous results also show that especially the width of the ribbon-like aggregates can also be varied by choice of the preparation conditions and the charge ratio between bile salt and block copolymer.

Clearly, we have only begun to explore the possibilities to vary the rich morphology of aqueous block copolymer–bile salt aggregates in a controlled way. In addition to varying the copolymer block lengths and the nature of the bile salt – possibilities that have not nearly been exhausted – our results suggest strategies to use deliberate polymer mixtures. For instance, replacing some of the block copolymer with a homopolymer of the polycation would inflate the aggregate core, and

using bidisperse block copolymers (two lengths of either the neutral or the cationic block, or both) would affect the curvature, and thus the shape, of the elongated aggregate. A more detailed investigation of how the life-time of metastable aggregates with disordered cores depend on the block copolymer block lengths is warranted, but also other variables, such as the content of simple salt in the dispersion, may be important.

Data availability

The data supporting this article have been included as part of the ESI.†

Conflicts of interest

There are no conflicts to declare.

Acknowledgements

The National Center for High Resolution Electron Microscopy (nCHREM) at Lund University is acknowledged for providing the access to the cryo-TEM facility. We are grateful to Crispin Hetherington for assisting with the cryo-TEM experiments at nCHREM. We thank Viveka Alfredsson for discussions. We would like to thank LNNano/CNPEM for the access to the cryo-TEM facility and technical support, in the execution of the proposal CRYO-EM-C2-20210263. Laura Caetano Escobar da Silva is acknowledged for her help with the cryo-TEM experiments. We are thankful to the São Paulo Research Foundation (FAPESP) for the financial support (grant numbers 2019/15956-9 and 2021/12071-6). S. G. T. thanks the Brazilian Agency CAPES (Finance Code 001) for the PhD scholarship and to INCT-Catálise/FAPESC/CNPq/CAPES, Brazil, for supporting her visit to Lund University, and W. L. thanks the Brazilian Agency CNPq for the senior researcher grant (grant number 306398/2018-4). We also acknowledge financial support from the Lund University/FAPESP (SPRINT) collaboration mobility project (to K. S.), The Swedish Research Council (K. S., grant number 2022-02860) and Magnus Bergwalls Stiftelse (K. S., grant number 2017-02225). G. D. acknowledges the China Scholarship Council (CSC) for the PhD scholarship (grant number 201706870015).

References

1 J. F. Berret, G. Cristobal, P. Hervé, J. Oberdisse and I. Grillo, *Eur. Phys. J. E*, 2002, **9**, 301–311.
2 S. Van Der Burgh, A. De Keizer and M. A. C. Stuart, *Langmuir*, 2004, **20**, 1073–1084.
3 I. K. Voets, A. de Keizer and M. A. Cohen Stuart, *Adv. Colloid Interface Sci.*, 2009, **147–148**, 300–318.
4 S. G. Trindade, L. Piculell and W. Loh, *Langmuir*, 2022, **38**, 2906–2918.
5 L. Shen, Y. Li, Q. Lu, X. Qi, X. Wu, Z. Zhou and J. Shen, *Chem. Commun.*, 2020, **56**, 2411–2414.
6 S. Bayati, K. E. Bergquist, K. Zhu, B. Nyström, J. Skov Pedersen, L. Galantini and K. Schillén, *J. Polym. Sci., Part B: Polym. Phys.*, 2017, **55**, 1457–1470.
7 J. R. Magana, C. C. M. Sproncken and I. K. Voets, *Polymers*, 2020, **12**, 1953.
8 Y. Anraku, A. Kishimura, M. Oba, Y. Yamasaki and K. Kataoka, *J. Am. Chem. Soc.*, 2010, **132**, 1631–1636.
9 H. M. Van Der Kooij, E. Spruijt, I. K. Voets, R. Fokkink, M. A. Cohen Stuart and J. Van Der Gucht, *Langmuir*, 2012, **28**, 14180–14191.
10 J. B. Sabadini, C. L. P. Oliveira and W. Loh, *Langmuir*, 2024, **40**, 2015–2027.
11 J. B. Sabadini, C. L. P. Oliveira and W. Loh, *J. Colloid Interface Sci.*, 2025, **678**, 1012–1021.
12 G. A. Ferreira, M. Ram-On, Y. Talmon, K. Schillén, L. Piculell and W. Loh, *Langmuir*, 2023, **39**, 4113–4124.
13 I. A. Van Hees, P. J. M. Swinkels, R. G. Fokkink, A. H. Velders, I. K. Voets, J. Van Der Gucht and M. Kamperman, *Polym. Chem.*, 2019, **10**, 3127–3134.
14 M. Uchman, M. Štěpánek, S. Prévost, B. Angelov, J. Bednár, M. S. Appavou, M. Gradzielski and K. Procházka, *Macromolecules*, 2012, **45**, 6471–6480.
15 M. Uchman, M. Gradzielski, B. Angelov, J. Oh and T. Chang, *Macromolecules*, 2013, **46**, 2172–2181.
16 L. Vitorazi, J. F. Berret and W. Loh, *Langmuir*, 2013, **29**, 14024–14033.
17 G. A. Ferreira, L. Piculell and W. Loh, *ACS Omega*, 2016, **1**, 1104–1113.
18 L. Galantini, M. C. di Gregorio, M. Gubitosi, L. Travaglini, J. V. Tato, A. Jover, F. Meijide, V. H. Soto Tellini and N. V. Pavel, *Curr. Opin. Colloid Interface Sci.*, 2015, **20**, 170–182.
19 D. Madenci and S. U. Egelhaaf, *Curr. Opin. Colloid Interface Sci.*, 2010, **15**, 109–115.
20 M. C. Di Gregorio, L. Travaglini, A. Del Giudice, J. Cautela, N. V. Pavel and L. Galantini, *Langmuir*, 2019, **35**, 6803–6821.
21 G. Du, D. Belić, A. Del Giudice, V. Alfredsson, A. M. Carnerup, K. Zhu, B. Nyström, Y. Wang, L. Galantini and K. Schillén, *Angew. Chem., Int. Ed.*, 2022, **134**, 1–8.
22 Y. Qiao, Y. Lin, Y. Wang, Z. Yang, J. Liu, J. Zhou, Y. Yan and J. Huang, *Nano Lett.*, 2009, **9**, 4500–4504.
23 K. Schillén, L. Galantini, G. Du, A. Del Giudice, V. Alfredsson, A. M. Carnerup, N. V. Pavel, G. Masci and B. Nyström, *Phys. Chem. Chem. Phys.*, 2019, **21**, 12518–12529.
24 M. C. Di Gregorio, M. Gubitosi, L. Travaglini, N. V. Pavel, A. Jover, F. Meijide, J. Vázquez Tato, S. Sennato, K. Schillén, F. Tranchini, S. De Santis, G. Masci and L. Galantini, *Phys. Chem. Chem. Phys.*, 2017, **19**, 1504–1515.
25 G. Du, A. Del Giudice, V. Alfredsson, A. M. Carnerup, N. V. Pavel, W. Loh, G. Masci, B. Nyström, L. Galantini and K. Schillén, *Polymer*, 2020, **206**, 122871.
26 S. Saeki, N. Kuwahara, M. Nakata and M. Kaneko, *Polymer*, 1976, **17**, 685–689.
27 G. Karlström, *J. Phys. Chem.*, 1985, **89**, 4962–4964.
28 Y. C. Bae, S. M. Lambert, D. S. Soane and J. M. Prausnitz, *Macromolecules*, 1991, **24**, 4403–4407.
29 A. Skandalis and S. Pispas, *Polym. Chem.*, 2017, **8**, 4538–4547.

30 A. Svensson, L. Piculell, B. Cabane and P. Ilekti, *J. Phys. Chem. B*, 2002, **106**, 1013–1018.
31 J. Janiak, S. Bayati, L. Galantini, N. V. Pavel and K. Schillén, *Langmuir*, 2012, **28**, 16536–16546.
32 C. L. P. Oliveira, M. A. Behrens, J. S. Pedersen, K. Erlacher, D. Otzen and J. S. Pedersen, *J. Mol. Biol.*, 2009, **387**, 147–161.
33 H. Amenitsch, H. Edlund, A. Khan, E. F. Marques and C. La Mesa, *Colloids Surf., A*, 2003, **213**, 79–92.
34 O. B. Ijare, B. S. Somashekar, Y. Jadegoud and G. A. N. Gowda, *Lipids*, 2005, **40**, 1031–1041.
35 G. A. Ferreira, W. Loh, D. Topgaard, O. Söderman and L. Piculell, *Polymers*, 2021, **13**, 3265.
36 V. Sharma, K. Park and M. Srinivasarao, *Proc. Natl. Acad. Sci. U. S. A.*, 2009, **106**, 4981–4985.
37 M. Boksebeld, N. P. Blanchard, A. Jaffal, Y. Chevolot and V. Monnier, *Gold Bull.*, 2017, **50**, 69–76.
38 C. L. Pinto Oliveira, *Current Trends in X-Ray Crystallography*, 2011.
39 A. Rich and D. Blow, *Nature*, 1958, **182**, 423–426.
40 A. A. D'Archivio, L. Galantini, E. Giglio and A. Jover, *Langmuir*, 1998, **14**, 4776–4781.
41 A. Naderi and P. M. Claesson, *J. Dispers. Sci. Technol.*, 2005, **26**, 329–340.
42 A. Naderi, P. M. Claesson, M. Bergström and A. Dedinaite, *Colloids Surf., A*, 2005, **253**, 83–93.
43 A. Mezei, R. Mészáros, I. Varga and T. Gilányi, *Langmuir*, 2007, **23**, 4237–4247.
44 E. Guzmán, L. Fernández-Peña, F. Ortega and R. G. Rubio, *Curr. Opin. Colloid Interface Sci.*, 2020, **48**, 91–108.
45 R. A. Campbell, A. Angus-Smyth, M. Yanez Arteta, K. Tonigold, T. Nylander and I. Varga, *J. Phys. Chem. Lett.*, 2010, **1**, 3021–3026.
46 A. Halperin, M. Kröger and F. M. Winnik, *Angew. Chem., Int. Ed.*, 2015, **54**, 15342–15367.
47 S. Saeki, N. Kuwahara, M. Nakata and M. Kaneko, *Polymer*, 1977, **18**, 1027–1031.
48 J. Zhang, H. Wang, X. Li, S. Song, A. Song and J. Hao, *J. Phys. Chem. B*, 2016, **120**, 6812–6818.
49 A. Jover, J. Troncoso, M. C. di Gregorio and F. Fraga López, *J. Mol. Liq.*, 2022, **361**, 119621.
50 A. A. D'Archivio, L. Galantini and E. Tettamanti, *J. Phys. Chem. B*, 2000, **104**, 9255–9259.
51 H. Sugioka, K. Matsuoka and Y. Moroi, *J. Colloid Interface Sci.*, 2003, **259**, 156–162.
52 C. Leggio, L. Galantini, E. Zaccarelli and N. V. Pavel, *J. Phys. Chem. B*, 2005, **109**, 23857–23869.
53 J. F. Berret, B. Vigolo, R. Eng, P. Hervé, I. Grillo and L. Yang, *Macromolecules*, 2004, **37**, 4922–4930.
54 J. F. Berret, *J. Chem. Phys.*, 2005, **123**, 164703.
55 F. Oesterhelt, M. Rief and H. E. Gaub, *New J. Phys.*, 1999, **1**, 6.1.
56 H. J. Kreuzer, R. L. C. Wang and M. Grunzez, *New J. Phys.*, 1999, **1**, 21.1.
57 D. Nguyen, X. F. Zhong, C. E. Williams and A. Eisenberg, *Macromolecules*, 1994, **27**, 5173–5181.
58 N. A. Lynd, A. J. Meuler and M. A. Hillmyer, *Prog. Polym. Sci.*, 2008, **33**, 875–893.
59 M. Asad Ayoubi, K. Zhu, B. Nyström, U. Olsson, K. Almdal, A. R. Khokhlov and L. Piculell, *J. Polym. Sci., Part B: Polym. Phys.*, 2013, **51**, 1657–1671.
60 G. A. Ferreira, L. Piculell and W. Loh, *Macromolecules*, 2018, **51**, 9915–9924.

